

# THE LOCAL VERTICAL DENSITY DISTRIBUTION OF ULTRACOOOL DWARFS M7 TO L2.5 AND THEIR LUMINOSITY FUNCTION

S.J. WARREN<sup>1</sup>, S. AHMED<sup>2</sup>, AND R.C. LAITHWAITE<sup>1</sup>

<sup>1</sup>Astrophysics Group, Imperial College London, Blackett Laboratory, Prince Consort Road, London SW7 2AZ, UK and  
<sup>2</sup>Centre for Electronic Imaging, School of Physical Sciences, The Open University, Walton Hall, Milton Keynes, MK7 6AA, UK

arXiv:2010.11093v1 [astro-ph.GA] 19 Oct 2020

We investigate the form of the local vertical density profile of the stars in the Galactic disk, close to the Galactic plane. We use a homogeneous sample of 34 000 ultracool dwarfs M7 to L2.5 that all lie within 350 pc of the plane. We fit a profile of the form  $\text{sech}^\alpha$ , where  $\alpha = 2$  is the theoretically preferred isothermal profile and  $\alpha = 0$  is the exponential function. Larger values of  $\alpha$  correspond to greater flattening of the profile towards the plane. We employ a likelihood analysis that accounts in a direct way for unresolved binaries in the sample, as well as for the spread in absolute magnitude  $M_J$  within each spectral sub-type (Malmquist bias). We measure  $\alpha = 0.29^{+0.12}_{-0.13}$ . The  $\alpha = 1$  (sech) and flatter profiles are ruled out at high confidence for this sample, while  $\alpha = 0$  (exponential) is included in the 95% credible interval. Any flattening relative to exponential is modest, and is confined to within 50 pc of the plane. The measured value of  $\alpha$  is consistent with the results of the recent analysis by Xiang et al. Our value for  $\alpha$  is also similar to that determined for nearby spiral galaxies by de Grijs et al., measured from photometry of galaxies viewed edge on. The measured profile allows an accurate determination of the local space density of ultracool dwarfs M7 to L2.5, and we use this to make a new determination of the luminosity function at the bottom of the main sequence. Our results for the luminosity function are a factor two to three lower than the recent measurement by Bardalez Gagliuffi et al., that uses stars in the local 25 pc radius bubble, but agree well with the older study by Cruz et al.

**Keywords:** Cool stars, Galactic structure

## 1. INTRODUCTION

The variation of the space density of stars in the disk of the Milky Way, in the vertical direction, i.e. perpendicular to the plane of the disk, and at the solar radius, approximates to an exponential distribution (Gilmore and Reid 1983) up to heights of 1 kpc. What happens close to the plane? Is there a density cusp, or does the exponential soften? We do not have a clear answer to this question for the Milky Way, but the density profile is often modelled by a  $\text{sech}^2$  distribution (e.g. Gould et al. 1996; Siegel et al. 2002; Ferguson et al. 2017; Bennett and Bovy 2019), which softens by a factor four relative to an exponential. A self-gravitating isothermal sheet has this equilibrium solution (Spitzer 1942; Camm 1950; van der Kruit and Searle 1981), and this may be why the  $\text{sech}^2$  distribution is popular, even though it is well known that the velocity dispersion of the stars in the disk depends on age.

In considering this question a useful flexible functional form for the density distribution as a function of height  $z$  from the plane, is the generalised sech distribution proposed by Van der Kruit (1988):

$$\rho(z) = 2^{-2/n} \rho_e \text{sech}^{2/n}(nz/2z_e), \quad (1)$$

where  $z_e$  is a scale height. With this parameterisation, the exponential, sech, and  $\text{sech}^2$  distributions correspond to  $n = \infty, 2$ , and 1 respectively.

For data analysis this representation is unsatisfactory, because we want to constrain the value of the parameter  $n$ , but it has an infinite range, causing difficulty in defining the prior. For this reason we prefer the form used by Dobbie and Warren (2020), who substitute  $\alpha = 2/n$ , so

the function becomes:

$$\rho(z) = 2^{-\alpha} \rho_e \text{sech}^\alpha(z/\alpha z_e), \quad (2)$$

and now the exponential, sech, and  $\text{sech}^2$  distributions correspond to  $\alpha = 0, 1, 2$ .

In this form, with different values of  $\alpha$ , the functions all have the same density at large values of  $|z|$  where they each asymptote to the exponential distribution with scale height  $z_e$ . The term  $2^{-\alpha}$  is therefore the degree of softening in the centre relative to the exponential distribution. This shows that the  $\text{sech}^2$  distribution softens by a factor four, as quoted above. Example functions, with  $\rho_e = 1$ , are plotted in Fig. 1 for values of  $\alpha = 0, 0.5, 1, 2$ , (top to bottom, respectively) and for a scale height  $z_e = 300$  pc, which is the canonical value for the Milky Way (e.g. Gilmore and Reid 1983; Jurić et al. 2008; Bochanski et al. 2010; Chang et al. 2011).

Beyond a few scale heights there is an excess in the tail, requiring a second population, of larger scale height. However in the current paper we are only concerned with the density distribution close to the plane, at heights  $|z| < 350$  pc, so we will assume a single population.

In the remainder of this paper we will use the following equivalent parameterisation of the density function:

$$\rho(z) = \rho_0 \text{sech}^\alpha(z/\alpha z_e) = \rho_0 \text{sech}^\alpha((z' + z_\odot)/\alpha z_e). \quad (3)$$

Here  $\rho_0$  is the density in the Galactic plane,  $z_\odot$  is the height of the Sun above the Galactic plane, and  $z' = z - z_\odot$  is the vertical height measured from the Sun. Because our analysis is confined to distances  $< 350$  pc we ignore any effect of variation of the stellar density with Galactic radius, because the scale length for this is so large,  $\sim 3$  kpc.

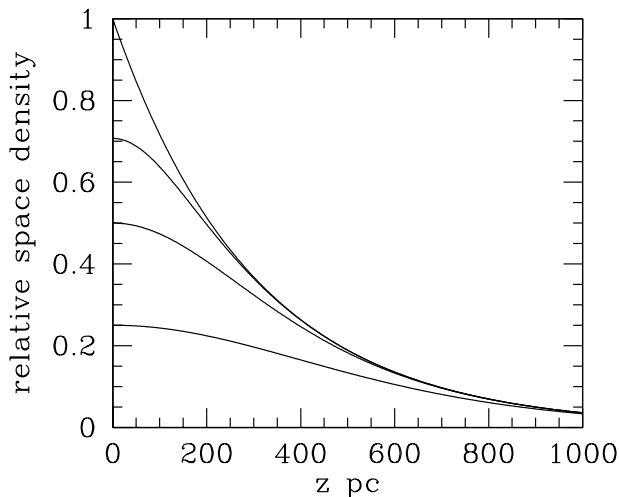


FIG. 1.— Density profiles, according to equation 2, with  $\rho_e = 1.0$  and  $z_e = 300$  pc. From top to bottom, the curves are: exponential,  $\text{sech}^{0.5}$ ,  $\text{sech}$ ,  $\text{sech}^2$ , which are  $\alpha = 0, 0.5, 1, 2$  respectively.

Dobbie and Warren (2020) summarise the status of measurements of  $\alpha$  in external galaxies and in the Milky Way. The best study of  $\alpha$  in external galaxies is the analysis by de Grijs et al. (1997) who measured the surface brightness profiles of edge-on spiral galaxies in the  $K$  band, to minimise the effects of extinction. From a sample of 24 galaxies they found a distribution of values of  $\alpha = 0.5 \pm 0.2$  (corrected for seeing and extinction), and they argue that the true value may be even lower due to a bias because the galaxies are not viewed perfectly edge on.

In the Milky Way itself there have been very few quantitative studies that contribute to this question. Using observations in the near-infrared Hammersley et al. (1999) state that “Analysis of one relatively isolated cut through an arm near longitude 65 degrees categorically precludes any possibility of a  $\text{sech}^2$  stellar density function for the disc.” In a footnote Jurić et al. (2008) state that the exponential profile provides a better fit than  $\text{sech}^2$  close to the plane. Using *Gaia DR1* Bovy (2017) draws a different conclusion. He measured the vertical density distribution separately for different spectral types A to K, and states “All vertical profiles are well represented by  $\text{sech}^2$  profiles, with scale heights ranging from  $\sim 50$  pc for A stars to  $\sim 150$  pc for G and K dwarfs and giants”. However, he does not fit  $\alpha$  as a free parameter and measure the uncertainty, so it is unclear what ‘well represented’ here means. Furthermore for the later-type stars the profile fits are not compelling. It is noteworthy that the measured scale heights are much smaller than the canonical value for the thin disk of 300 pc, even for the later-type stars for which one might expect agreement.

The most detailed information on the vertical density distribution is provided by the recent study by Xiang et al. (2018) using LAMOST spectroscopic observations. They are able to divide stars into several age bins. The measured values of  $\alpha = 2/n_1$  (their Table 3b) show sig-

nificant differences between age bins, both up and down, but averaging over several bins one can see that the younger populations, ages  $< 8$  Gyr, have smaller scale heights and average  $\alpha \sim 1$ , while the older populations, ages  $> 8$  Gyr, have larger scale heights and  $\alpha \sim 0$ . Combining all ages together the best fit value is also  $\alpha \sim 0$ . The selection function for this survey is exceedingly complex, and the estimation of  $\alpha$  was not a primary aim of the project. The significant variations in  $\alpha$  between different age bins may indicate that the uncertainties have been underestimated, which is why we have not quoted uncertainties here. Nevertheless the overall trend of  $\alpha$  decreasing with age seems clear and this is the first time that this has been shown.

In their own study, Dobbie and Warren (2020) used the large samples of K and M stars from SDSS collated by Ferguson et al. (2017) to study the problem. They found that there is moderate evidence (specifically meaning  $2 < \ln B < 5$ , where  $B$  is the Bayes factor) for the exponential and  $\text{sech}$  models over the  $\text{sech}^2$  model, but concluded that a sample that reaches closer to the Galactic plane is needed. This is in fact the problem with the majority of samples of the vertical structure of the Galactic disk, that they sample a conical volume, with the Sun at the apex, so the space density at small heights  $|z| < 300$  pc is not sufficiently well sampled, if at all. This may be compounded by the problem that the images of nearby stars are saturated.

The results on  $\alpha$  of Xiang et al. (2018) and Dobbie and Warren (2020) are not in agreement with the finding of Bovy (2017) that  $\alpha \sim 2$ . As with the study of Xiang et al. (2018), the selection function for the sample of Bovy (2017) is rather complex. This makes it very difficult to investigate the origin of the disagreement. These results motivate a new measurement of  $\alpha$  using a survey with good sampling of the local volume, distances  $< 500$  pc, with a simple selection function, and ideally selected at near-infrared wavelengths to minimise extinction. In this paper we analyse such a sample: we combine 32 942 M7 to M9.5 dwarfs from Ahmed and Warren (2019) with 1 016 L0 to L2.5 dwarfs from Skrzypek et al. (2016), all selected from UKIDSS, to measure an accurate value of  $\alpha$ . This in turn provides a measurement of the space density of each spectral type in the plane of the disk, which can be transformed to the luminosity function at the bottom of the main sequence.

The layout of the remainder of the paper is as follows. In Sect. 2 we describe the samples used in the analysis. In Sect. 3 we analyse the vertical density distribution using firstly a binned estimate, and then a maximum-likelihood fit using every star individually. We provide a discussion of these results on the vertical density distribution in Sect. 4. In Sect. 5 we use the results to determine the stellar luminosity function over the spectral range M7 to L2.5. We provide a summary of the main points in Sect. 6. All magnitudes in this paper are on the Vega system. The  $J$  band refers to the MKO  $J$  passband (Tokunaga et al. 2002), unless specifically stated otherwise.

## 2. SAMPLES

By combining the samples of Ahmed and Warren (2019) and Skrzypek et al. (2016) we create a large homogeneous sample of 33 958 M7 to L2.5 dwarfs  $13.0 <$

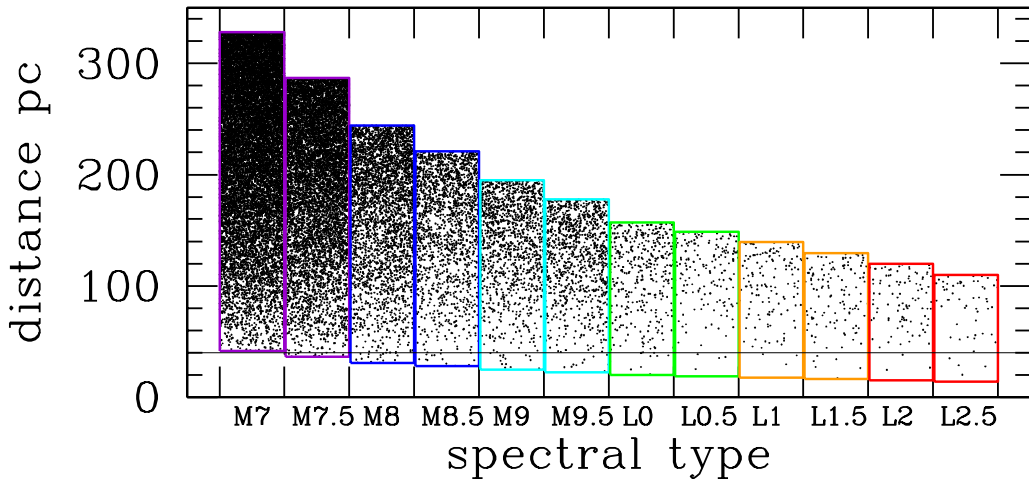


FIG. 2.— Distribution of distances for the sample of 33 985 M7 to L2.5 dwarfs, where for this plot sources are treated as single (unresolved binaries are ignored). For each spectral type the upper and lower distance limits correspond to the sample magnitude limits  $13.0 < J < 17.5$ . The sample is complete over all spectral types between distances  $d_{\min}(\text{M7})$  and  $d_{\max}(\text{L2.5})$ , which is the range  $41.3 < d < 109.5$  pc. The thin horizontal line is drawn at a distance of 40 pc, to make clear the relative contributions of the different spectral sub-types to measuring the space density at very small distances.

$J < 17.5$ , at distances  $< 350$  pc (except for unresolved binaries as explained below). The hydrogen burning limit is believed to be reached after spectral type L2.5 (Dieterich et al. 2014), meaning that L3 dwarfs and later are brown dwarfs, while L2.5 dwarfs and earlier are predominantly main sequence stars, but can also include young brown dwarfs. In the field the proportion of young brown dwarfs is small, and therefore the sample of M7 to L2.5 dwarfs is representative of the bottom of the main sequence. The numbers of dwarfs of different spectral types are listed in Table 1. As detailed in the above catalogue papers these samples are well suited to measuring the density profile and the luminosity function. The samples are highly complete, and the spectral classifications are unbiased except for rare peculiar blue or red sources, comprising an estimated  $\sim 1\%$  of the sample.

The two samples cover the same area of sky and were selected by essentially identical methods using the *phototype* method of Skrzypek et al. (2015). The method classifies objects using multicolour photometry. For the L dwarfs the bands *izYJHKW1W2* were used, while for the M dwarfs the W1 and W2 bands were omitted. They add no significant useful information for these types. The accuracy of the spectral types is competitive with spectroscopy. For the M dwarfs the classification is accurate to better than 0.5 sub-types *rms*, and is tied to the optical spectroscopy of the BOSS sample of Schmidt et al. (2015). For the L dwarfs the classification is accurate to one sub-type *rms*, and is anchored to the optical system of Kirkpatrick et al. (1999). The sample is presented in Fig. 2, where each star has been plotted at the distance computed assuming that the object is single (ignoring unresolved binaries). The sample is plotted in a different way in Fig. 3, as a histogram showing heights from the Galactic plane, assuming the Sun lies at a height of 10 pc above the plane. This plot illustrates the fact that the sample includes a large number of objects at heights

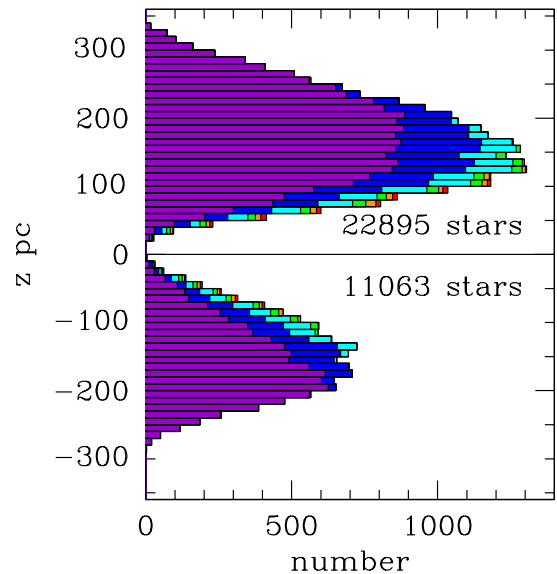


FIG. 3.— Distribution of height  $z$  above the Galactic plane for the sample, coloured by spectral type: M7+M7.5 (purple), M8+M8.5 (blue), M9+M9.5 (cyan), L0+L0.5 (green), L1+L1.5 (orange), L2+L2.5 (red). For this plot the Sun is assumed to lie at a height of 10 pc above the plane.

$|z| < 100$  pc, and therefore is well suited to investigating the softening close to the Galactic plane. The survey covers an effective area of  $3031 \text{ deg}^2$  (7.3% of the sky), and the solid angle as a function of Galactic latitude  $\Omega(b)$  is provided in Table 1 of Ahmed and Warren (2019), in wedges of angular extent  $1^\circ$ . The sample defined in this way has excluded from the slightly larger total sample

TABLE 1  
NUMBER OF SOURCES AND ABSOLUTE MAGNITUDE  
BY SPECTRAL TYPE

SpT	Count	$M_J$	SpT	Count	$M_J$
M7	15 772	9.92	L0	408	11.52
M7.5	9 242	10.21	L0.5	175	11.64
M8	3 637	10.56	L1	143	11.78
M8.5	1 851	10.78	L1.5	130	11.94
M9	1 354	11.05	L2	103	12.11
M9.5	1 086	11.25	L2.5	57	12.30
total	32 942		total	1 016	

two small areas of larger reddening, totalling 39 deg<sup>2</sup>.

The photometry for this sample is very precise and extinction is very low. In the  $J$  band the median photometric uncertainty is 0.016, and the 90% quantile is 0.028. We quantify the extinction using the results from Green et al. (2018), for a distance of 400 pc. This is an overestimate of the effects of dust on the sample, but the method of Green et al. (2018) becomes too inaccurate at smaller distances to be useful. On this basis in the  $J$  band the median extinction is  $< 0.02$  mag. and for 90% of sources the extinction is  $< 0.06$  mag. For only 0.3% of the sources is the extinction at 400 pc greater than 0.13 mag. Therefore we make no corrections for extinction.

Laithwaite and Warren (2020) have made a detailed study of the unresolved binaries in the sample of M7 to M9.5 dwarfs. They find that unresolved binaries comprise 16.2% of all the systems, and that the binaries are almost exclusively equal mass systems. This means that we can assume that per unit volume 16.2% of the sources are twice as bright as single stars. We will assume that the same properties apply to the L0 to L2.5 dwarfs. In this respect we note that Reid et al. (2008) find a similar fraction of unresolved binaries in their sample of L dwarfs.

Laithwaite and Warren (2020) also redetermined values of the absolute magnitude  $M_J$  for spectral types M7 to M9.5, based on *Gaia* parallaxes, finding values some 0.5 mag. brighter than those of Dupuy and Liu (2012). The new values are listed in Table 1. The distances quoted in Ahmed and Warren (2019) used the absolute magnitudes of Dupuy and Liu (2012) and are therefore wrong. The reasons for the discrepancy are not due to incorrect parallaxes in Dupuy and Liu (2012) but appear to be due to differences in spectral classifications between different samples. The sample of Ahmed and Warren (2019) is homogeneous and the classifications are accurately calibrated to the classifications of the BOSS spectroscopic sample of Schmidt et al. (2015), which itself is homogeneous and was subject to careful checks for systematics. The sample of Schmidt et al. (2015) has become the *de facto* standard in this field, but the above apparent discrepancy in spectral classifications needs to be borne in mind when comparing results derived from different samples.

For the L0 to L2.5 stars the absolute magnitudes in Table 1 were calculated using the polynomial relation between  $M_J$  and spectral type of Dupuy and Liu (2012), derived from ground-based parallaxes. We checked these values by first matching to *GAI*A all the L0 to L3 dwarfs in the sample of Skrzypek et al. (2016), then limiting to sources with  $\text{parallax}/\text{error} > 10$ . We then fit a linear

relation between absolute magnitude and spectral type, allowing for binaries by fitting a double Gaussian profile to the distribution of absolute magnitudes at fixed spectral type. The method is very similar to that employed by Laithwaite and Warren (2020) for the M7 to M9.5 stars, except they used  $G - J$  colour rather than spectral type. The result for single stars is the linear relation  $M_J = 0.359 \text{ SpT} + 7.882$  where SpT denotes spectral type and L0, L3 are 10, 13<sup>1</sup>. Comparing against the values in Table 1 we find agreement at the level  $|\Delta M_J| < 0.1$  for all sub-types L0 to L2.5, confirming that the absolute magnitudes of Dupuy and Liu (2012) are reliable over this spectral range.

### 3. FITTING THE VERTICAL DENSITY DISTRIBUTION

It is usual to measure the density distribution by first binning the data and then fitting to the counts. This is useful because the binned counts give a visual impression of the shape of the variation in density. There is an important drawback to this approach however, in that it is unclear how to deal with the binaries: in Fig. 2 the binaries (which cannot be identified individually) should be plotted at a distance a factor  $\sqrt{2}$  larger. Here we first present a binned analysis of the M7 and M7.5 stars only, which includes a large fraction of all the stars, and we then provide results of an optimal method that fits to all the data points simultaneously, without binning, and correctly accounts for binaries.

#### 3.1. Binned analysis

In this section we simply ignore the fact that a fraction of the sources are unresolved binaries, and treat all the sources as single. The results are illustrative and used as a guide to the more complete analysis presented in the next subsection. Referring to Fig. 2 the lower and upper distance limits for each spectral type correspond to the magnitude limits of the survey  $J = 13.0$  and 17.5, given the absolute magnitude for any particular spectral type. Therefore we can form a volume-complete sample of M7 and M7.5 stars by using distance limits  $d_{min}(M7)$ , and  $d_{max}(M7.5)$ , which are 41.3 pc and 287.1 pc respectively. The sample comprises 20 849 stars and is plotted in Fig. 4 using polar coordinates. The blue histogram plots the solid angle of the survey at each value of  $b$ , in 1° wedges. Therefore to compute the space density we sum the number of sources in each slice, of height 10 pc, and sum the volume contributed by each wedge along the slice, accounting for the solid angle as it varies with  $b$ . For this calculation we assume the Sun lies at a height of 10 pc above the Galactic plane.

The results of this calculation are plotted in Fig. 5. The blue points are the binned estimates of space density at heights above the plane, and the red points are the same for below the plane. The uncertainty on each point is plotted as a fractional uncertainty of  $1/\sqrt{N}$ , where  $N$  is the number of points in the slice, and we have only used bins with  $> 20$  points. The grey points are the blue points reflected about the Galactic plane, and allow a comparison of the variation in space density above and below the plane. There are no strong differences between

<sup>1</sup> Beware that others, e.g. Bardalez Gagliuffi et al. (2019), use 20, 23 for L0, L3.

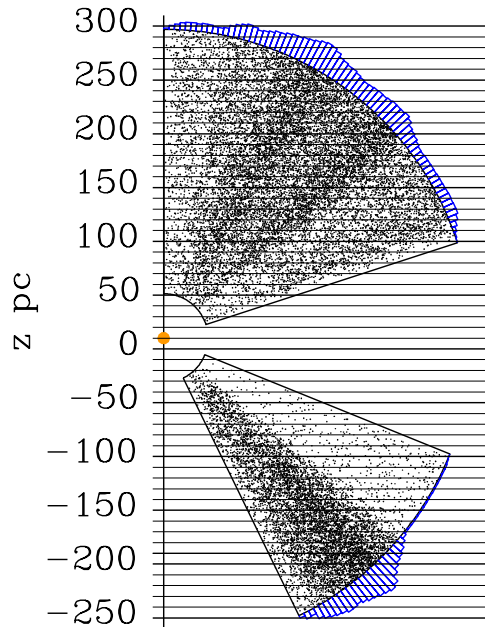


FIG. 4.— Polar plot, with coordinates distance  $d$  and Galactic latitude  $b$ , for the volume-complete sample of 20 849 M7 and M7.5 stars with distances between  $d_{\min}(\text{M7}) = 41.3$  pc and  $d_{\max}(\text{M7.5}) = 287.1$  pc. The blue histogram shows the areal coverage, with the radial length of each bin proportional to the solid angle at that  $b$ . The orange dot indicates the observer, located 10 pc above the Galactic plane. The horizontal slices are those used in the binned estimates of the space density.

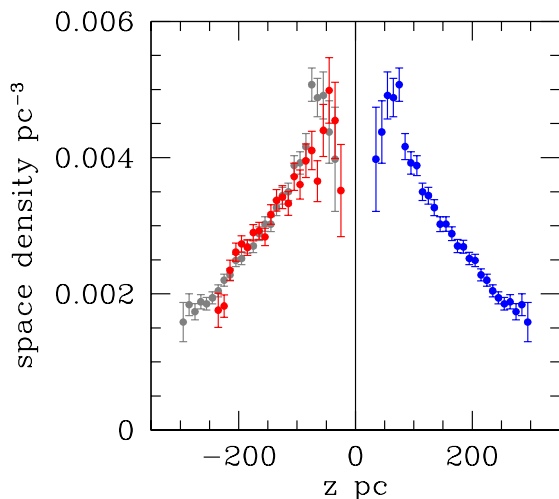


FIG. 5.— Binned estimate of the variation of space density with height  $z$  above the Galactic plane, for the volume-complete sample of 20 849 M7 and M7.5 stars with distances  $41.3 < d < 287.1$ . Red points - below the plane; blue points - above the plane; grey points - the blue points reflected through the origin.

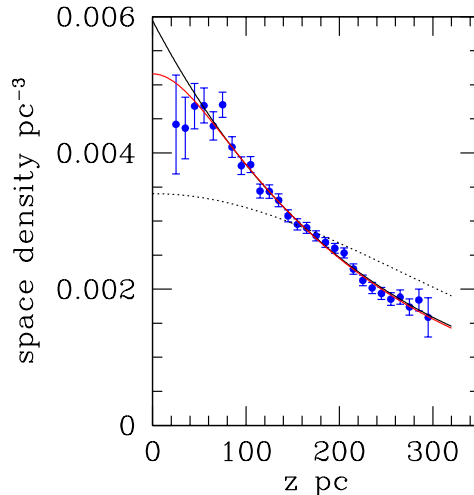


FIG. 6.— Binned estimate of the variation of space density with absolute height  $|z|$  above the Galactic plane, for the volume-complete sample of 20 849 M7 and M7.5 stars with distances  $41.3 < d < 287.1$  pc. Red curve: best fit  $\text{sech}^\alpha$  with  $\alpha = 0.23$ . Black curve: best fit exponential. Dotted curve: best fit  $\text{sech}^2$  with scale height  $z_e$  fixed to 200 pc.

the two curves, indicating consistency. It well known that at larger distances from the plane differences are seen when comparing measurements above and below the plane (e.g. Widrow et al. 2012; Ferguson et al. 2017). It is possible that density fluctuations exist at a similar level in our data but they would be relatively less important close to the Galactic plane where the space densities are higher. Given the good agreement between the red and the grey points we are justified in averaging the results for above and below the plane. The averaged results are presented in Fig. 6.

In fitting a model to the data, we assume Gaussian errors for each bin i.e. we approximate the Poisson distribution as Gaussian. Then if the model predicts  $m_i$  points in bin  $i$ , and the observed number is  $n_i$ , the logarithm of the likelihood is given by:

$$\ln \mathcal{L} = - \sum \frac{(n_i - m_i)^2}{2m_i} - \frac{1}{2} \sum \ln m_i, \quad (4)$$

which is Eqn 8 in Dobbie and Warren (2020). Because the likelihood is strongly peaked in the space of the parameters, the posterior is not sensitive to the form of the priors. We adopt broad uniform priors, which for the shape parameter covers the range  $0 < \alpha < 3$ . The function  $\text{sech}^\alpha(z/\alpha z_e)$  can be awkward to evaluate for small values of  $\alpha$ , so we employ the identity

$$\text{sech}^\alpha(x/\alpha) = 2^\alpha e^{-x} (1 + e^{-2x/\alpha})^{-\alpha}, \quad (5)$$

and ensure that when  $\alpha = 0$  the function is set equal to  $e^{-x}$ .

Fitting Eqn 3, we measure  $\alpha = 0.23 \pm 0.13$ , and  $z_e = 222^{+8}_{-10}$  pc. This quantifies that the density profile is consistent with exponential all the way to the Galactic plane and that any flattening is modest. The best-fit profile is plotted in Fig. 6, where it is compared to the best-fit exponential, which has a scale height  $z_e = 227^{+7}_{-6}$  pc. This

indicates that any softening is confined to within 50 pc of the plane. The data are inconsistent with not only the  $\text{sech}^2$  profile, but also the sech profile. Interestingly fitting a  $\text{sech}^2$  profile, which is a bad fit, yields a scale height of 126 pc which makes no sense when compared to the fiducial scale height of the thin disk of 300 pc. This calculation shows that force-fitting the wrong profile, one that flattens too much in the centre, leads to an underestimate of the correct scale height. The problem of the  $\text{sech}^2$  profile may be illustrated in another way. Because we have not accounted for binaries the binned analysis underestimates the true scale height somewhat. If we suppose that the scale height, uncorrected for binaries, could be as small as  $z_e = 200$  pc, and fit a  $\text{sech}^2$  profile with this scale height the result is the very flattened and clearly incorrect profile plotted as the dotted line in Fig. 6.

This binned analysis indicates that the profile is peaky near the centre, but the values of the fitted parameters are not correct because we have ignored the presence of unresolved binaries. It is well known that the presence of unresolved binaries in a sample causes the scale height to be underestimated, and conceivably it could affect the estimate of  $\alpha$  as well. The effect of unresolved binaries is usually quantified by modelling (e.g. Covey et al. 2008; Jurić et al. 2008; Bochanski et al. 2010). For example in the current case a synthetic catalogue would be created, one that includes unresolved binaries and that matches the selection criteria of the actual catalogue. The catalogue would be created with a scale height that is a guess for the true scale height and would be analysed in the same way as the actual sample. The catalogue scale height would then be adjusted until the measured (biased) scale height matches the measured value in the actual catalogue. In this way the true scale height is recovered.

In the next subsection we describe a likelihood analysis that instead accounts for unresolved binaries in a direct way, and makes additional improvements over the binned analysis presented in this section.

### 3.2. Full likelihood analysis

#### 3.2.1. Method

We now implement four improvements compared to the above binned analysis. These are:

1. Using stars individually without binning.
2. Accounting correctly for the presence of unresolved binaries.
3. Accounting for the intrinsic spread in absolute magnitude  $M_J$  of each spectral type, which in a magnitude-limited sample means that intrinsically brighter sources are over-represented – the Malmquist bias.
4. Including all stars in the sample from M7 to L2.5 over the full distance range of each type (displayed in Fig. 2).

We wish to calculate the likelihood  $\mathcal{L}$  of observing the sample in question. In deriving this we will assume a Poisson point process, and follow a similar procedure to

that presented by Marshall et al. (1983). Consider firstly a single spectral sub-type  $t$ . The data comprise the list of sources of observed Galactic latitude  $b$  and apparent magnitude  $J$ . Ignoring binaries, the expected number of sources  $\mu$  in an infinitesimal element  $dbdJ$  is:

$$\mu = \rho(z(d(J), b, z_\odot)) d^2(J) \Omega(b) db \frac{dd}{dJ} dJ. \quad (6)$$

Here, and throughout this section,  $d(J)$  refers to the distance of a single star computed from  $J$  using the absolute magnitude for the particular sub-type, listed in Table 1. The height above the plane is calculated as  $z(d(J), b, z_\odot) = d(J) \sin(b) + z_\odot$ . The angle  $b$  is in degrees, since  $\Omega(b)$  is the solid angle defined in wedges of angular size  $1^\circ$  (see Sect. 2). The term  $\rho(z(d(J), b, z_\odot))$  should be understood to include the dependence on the model parameters  $\rho_0(t)$ ,  $z_e$  and  $\alpha$ .

The probability of finding one source in the element is  $\mu e^{-\mu}$ , and of finding none is  $e^{-\mu}$ . Therefore the likelihood is the product of the probabilities of observing the  $N$  sources with their particular  $b, J$ , and of observing no sources in all the other elements. Consequently the likelihood for this type  $t$  may be written:

$$\mathcal{L}_t = \prod_i \mu_i e^{-\mu_i} \prod_j e^{-\mu_j}, \quad (7)$$

where the first product is over elements containing sources, and the second product is over all the other elements within the volume surveyed. Taking the logarithm and dropping terms that are independent of the model parameters we obtain:

$$\ln \mathcal{L}_t = \sum_i \ln(\rho(z(d(J_i), b_i, z_\odot)) - \iiint_V \rho dV, \quad (8)$$

and the volume integral is the expected number of sources in the survey, given the density function  $\rho$ , which depends on  $\rho_0(t)$ ,  $z_e$ ,  $\alpha$  and  $z_\odot$ . The likelihood as defined above uses all the stars of a particular sub-type individually, and deals with the first item above.

We now consider the treatment of binaries. It is relatively easy to treat the binaries correctly through the likelihood because we can assume that each binary is exactly twice as bright as a single, based on the detailed study of binaries in this sample by Laithwaite and Warren (2020). This means that the survey is in fact two surveys, one for singles, and a second for binaries, where the distance limits for the binary survey are  $\sqrt{2}$  larger than for the singles survey. For a total number of systems comprising a fraction  $f_b$  of unresolved equal-mass binaries, and so a fraction  $1 - f_b$  singles, if the space density of stars at any point is  $\rho$ , the space density of single stars is  $\rho(1 - f_b)/(1 + f_b) = \rho r_s$ , and the space density of binary systems  $\rho f_b/(1 + f_b) = \rho r_b$ . The binary systems are unresolved sources that are twice as bright as single stars, and we assume  $f_b = 0.162$  (Laithwaite and Warren 2020).

Returning now to equation 6, in computing the expected number of sources in an element  $dbdJ$  we must include the expected number of binary systems, and the

equation becomes:

$$\mu = [r_s \rho(z(d(J), b, z_\odot)) + 2\sqrt{2}r_b \rho(z(\sqrt{2}d(J), b, z_\odot))] \times d^2(J) \Omega(b) db \frac{dd}{dJ} dJ, \quad (9)$$

where the term  $2\sqrt{2}$  in front of  $r_b$  derives from the larger volume element at the larger distance (from the terms  $d$  and  $dd/dJ$ ). Propagating through to the logarithm of the likelihood, we obtain the final expression

$$\ln \mathcal{L}_t = \sum_i \ln [r_s \rho(z(d(J_i), b_i, z_\odot)) + 2\sqrt{2}r_b \rho(z(\sqrt{2}d(J_i), b_i, z_\odot))] - \iiint_V r_s \rho dV_s - \iiint_V r_b \rho dV_b, \quad (10)$$

where the first triple integral is over the volume occupied by singles, given the sample magnitude limits, and the second volume integral is the same for the binary systems, for which all distances are  $\sqrt{2}$  larger. In this way binaries are correctly included in the calculation of the likelihood.

We now consider how to treat Malmquist bias. Our sample is magnitude limited  $13.0 < J < 17.5$ . But (single or binary) stars of a particular spectral type have a spread in absolute magnitude (due to e.g. variations in age and/or metallicity). Therefore the more luminous sources are detected to larger distances, and are overrepresented in the sample, and *vice versa* for less luminous sources. If stars of a particular sub-type are treated as having a unique absolute magnitude the measured parameters of the density distribution will be biased, and this is what we mean when using the term Malmquist bias in this paper. Laithwaite and Warren (2020) found a Gaussian distribution of absolute magnitude of dispersion  $\sigma_M = 0.21$  mag. at fixed  $G - J$  colour. Over the colour spread of half a spectral sub-type the dispersion increases to  $\sigma_M = 0.24$  mag. which is the value we adopt. The additional dispersion comes from the relation between absolute magnitude and colour.

Eqn 10 shows us how to deal with the spread in the absolute magnitudes  $M_J$  of each spectral type. In Eqn 10 we are dealing with two populations, singles and binaries, where the binaries are twice as bright and occupy a different volume to the singles, where all distances are  $\sqrt{2}$  larger. In the same way each of these two populations comprises a set of sub-populations of different absolute magnitude, the more luminous sources occupying a volume where all distances are multiplied by a factor  $f > 1$ , compared to the average, and the less luminous sources occupying a volume where all distances are multiplied by their own factor  $f < 1$ . To implement this we divide each population (singles or binaries) into a small number of sub-populations, i.e. we model the Gaussian distribution of  $M_J$  as a coarse histogram. Each sub-population of absolute magnitude  $M_J - \Delta M_J$  has a distance correction  $f = 10^{0.2\Delta M_J}$  and a volume correction  $f^3$ , analogous to the  $\sqrt{2}$  and  $2\sqrt{2}$  terms in the second term in Eqn 10. For a set of subpopulations defined by weights  $w_j$  ( $\sum_j w_j = 1$ ) and distance corrections  $f_j$ , then, for ex-

TABLE 2  
BEST FIT VALUES AND THEIR UNCERTAINTIES FOR THE FULL LIKELIHOOD ANALYSIS

parameter	sech $^\alpha$	exponential
$\rho_0$ M7 pc $^{-3}$	$2.37^{+0.14}_{-0.09} \times 10^{-3}$	$2.79^{+0.06}_{-0.05} \times 10^{-3}$
$\rho_0$ M7.5	$1.88^{+0.12}_{-0.07} \times 10^{-3}$	$2.22^{+0.04}_{-0.04} \times 10^{-3}$
$\rho_0$ M8	$1.09^{+0.06}_{-0.03} \times 10^{-3}$	$1.28^{+0.03}_{-0.03} \times 10^{-3}$
$\rho_0$ M8.5	$0.71^{+0.05}_{-0.03} \times 10^{-3}$	$0.84^{+0.02}_{-0.02} \times 10^{-3}$
$\rho_0$ M9	$0.71^{+0.04}_{-0.03} \times 10^{-3}$	$0.83^{+0.03}_{-0.02} \times 10^{-3}$
$\rho_0$ M9.5	$0.72^{+0.05}_{-0.03} \times 10^{-3}$	$0.85^{+0.02}_{-0.03} \times 10^{-3}$
$\sum \rho_0$ M7-M9.5	$7.48^{+0.44}_{-0.28} \times 10^{-3}$	$8.80^{+0.15}_{-0.15} \times 10^{-3}$
$\rho_0$ L0	$0.38^{+0.03}_{-0.02} \times 10^{-3}$	$0.44^{+0.02}_{-0.02} \times 10^{-3}$
$\rho_0$ L0.5	$0.19^{+0.02}_{-0.02} \times 10^{-3}$	$0.22^{+0.02}_{-0.02} \times 10^{-3}$
$\rho_0$ L1	$0.18^{+0.02}_{-0.02} \times 10^{-3}$	$0.21^{+0.02}_{-0.02} \times 10^{-3}$
$\rho_0$ L1.5	$0.20^{+0.02}_{-0.02} \times 10^{-3}$	$0.23^{+0.02}_{-0.02} \times 10^{-3}$
$\rho_0$ L2	$0.20^{+0.02}_{-0.02} \times 10^{-3}$	$0.23^{+0.02}_{-0.02} \times 10^{-3}$
$\rho_0$ L2.5	$0.14^{+0.02}_{-0.02} \times 10^{-3}$	$0.16^{+0.02}_{-0.02} \times 10^{-3}$
$\sum \rho_0$ L0-L2.5	$1.29^{+0.08}_{-0.06} \times 10^{-3}$	$1.50^{+0.05}_{-0.05} \times 10^{-3}$
$\sum \rho_0$ M7-L2.5	$8.77^{+0.51}_{-0.32} \times 10^{-3}$	$10.30^{+0.16}_{-0.16} \times 10^{-3}$
$z_e$ pc	$258.6^{+10.2}_{-12.3}$	$269.3^{+6.6}_{-6.3}$
$\alpha$	$0.29^{+0.12}_{-0.13}$	...
$z_\odot$ pc	$10.9^{+1.7}_{-1.6}$	$10.0^{+1.5}_{-1.4}$

ample, the first term in Eqn 10,  $r_s \rho(z(d(J_i), b_i, z_\odot))$ , is replaced by  $r_s \sum_j w_j f_j^3 \rho(z(f_j d(J_i), b_i, z_\odot))$ . There is a similar sum for the second term, and then a set of volume integrals for all the sub-populations, single as well as binary, over the relevant volume occupied by each sub-population.

In principle photometric errors can have an effect that is similar to the effect of the spread in absolute magnitudes, but this can be safely ignored for this dataset as the photometric errors in the  $J$  band (Sect. 2) are considerably smaller than the dispersion in absolute magnitude.

The final improvement we make ensures that all the stars in the full sample are used, over the full distance range of each spectral sub-type (see Fig. 2), rather than limiting to the distance range in common, as we did in the binned analysis for the M7 and M7.5s. This can be achieved straightforwardly by assuming that the density function has the same form for each spectral sub-type, meaning that the parameters  $z_e, \alpha, z_\odot$  are in common, but the normalisations are different, i.e. the central space density of each spectral type is a free parameter  $\rho_0(t)$ . Then the likelihood is the sum of the individual likelihoods for each sub-type,  $\ln \mathcal{L} = \sum_t \ln \mathcal{L}_t$ , where the individual likelihoods are computed over the full sample and full volume for that sub-type. This means that the total number of free parameters is 15: the 12  $\rho_0(t)$ , and  $z_e, \alpha, z_\odot$ . To be completely clear:  $\rho_0(t)$  is the summed number of stars (not systems) per unit volume for a particular sub-type.

We adopt broad uniform priors on the parameters. Again, because the likelihoods are sharply peaked, the results are insensitive to the priors.

### 3.2.2. Results

We have fit the function  $\text{sech}^\alpha$ , as well as the simpler exponential function. We used the MCMC package `emcee` (Foreman-Mackey et al. 2013) to maximise the likelihood, and to measure the uncertainties. The results for both functions are summarised in Table 2, in

each case accounting for binaries and Malmquist bias in the analysis. The uncertainties quoted correspond to the 16, 50, 84% quantiles in the marginalised distributions, and for all the  $\rho_0(t)$  the fractional uncertainties are larger than  $1/\sqrt{N}$ . The uncertainties on the  $\rho_0(t)$  parameters are considerably larger for the  $\text{sech}^\alpha$  function compared to the exponential function because they include the uncertainty in the flattening towards the plane. We use the  $\text{sech}^\alpha$  results when comparing against local measurements of space densities, and in calculating the luminosity function. The exponential function fit is included because of its simplicity, and it can be used for comparison against other surveys except close to the plane  $|z| < 50$  pc.

The uncertainties on the  $\rho_0(t)$  parameters are highly correlated. Therefore when we perform arithmetic on the space densities (e.g. the summed space density of spectral types M7-M9.5 listed in Table 2, and later the calculation of the luminosity function), to measure the uncertainties we first perform the arithmetic on the MCMC chains and then measure the dispersion in the resulting chain.

A corner plot for the parameters  $\rho_0$  for the M7s,  $z_e$ ,  $z_\odot$ , and  $\alpha$  is presented in Fig. 7, produced using the `GetDist` package (Lewis 2019). We have included only one  $\rho_0(t)$  in this plot as the correlations for  $\rho_0(t)$  of the other spectral sub-types have a similar form.

The most interesting result, and the principal result of this paper, is the distribution for  $\alpha$ . As listed in Table 2 we measure  $\alpha = 0.29^{+0.12}_{-0.13}$ . Although the  $\alpha$  distribution is strongly peaked near 0.3, there is a shoulder to the distribution that extends to  $\alpha = 0$ . This shoulder reflects the fact that the data have almost no constraining power over the range  $0 < \alpha < 0.1$  because within this range the density distribution varies only very close to the plane  $|z| < 20$  pc, where there are very few sources, so the posterior is quite flat over this range. Quantifying the credible interval by the integrated probability within a range between equal probability densities, we find the 95% and 99% credible intervals are  $0 < \alpha < 0.50$  and  $0 < \alpha < 0.59$ , meaning that the  $\text{sech}$  profile,  $\alpha = 1$ , is firmly excluded. We wish to quantify at what level the credible interval includes the exponential model. This is ambiguous because the posterior density rises slightly as  $\alpha$  approaches zero (Fig. 7). A useful measure is to state the credible interval at which the range becomes one sided, i.e. once the full range of  $\alpha$  from the peak down to  $\alpha = 0$  is included, and this is the 95% interval. This means there is moderate evidence against the exponential model continuing all the way to the Galactic plane, or equivalently moderate evidence for some degree of flattening close to the plane. We compare the exponential and  $\text{sech}^\alpha$  fits in Fig. 8, plotting the summed density for the full spectral range M7 to L2.5. The two curves are essentially identical except at heights  $|z| < 50$  pc. Any softening of the exponential profile is rather slight.

We can quantify the effects of the different improvements implemented in the full likelihood analysis. For the binned data we had the pair of results for the scale height  $z_e$  and the shape parameter  $\alpha$  of [222, 0.23]. Implementing successively a) treating all points individually rather than binned, and over the full distance ranges for each sub-type, b) accounting for binaries, c) accounting

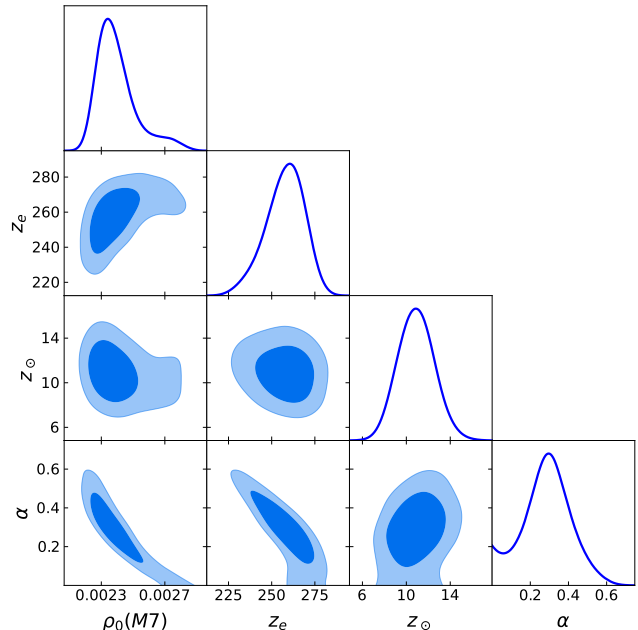


FIG. 7.— Corner plot of the posterior probability density for the parameters: central density  $\rho_0$  for the M7s, the scale height  $z_e$ , the offset of the Sun from the plane  $z_\odot$ , and the shape parameter  $\alpha$ . The contours contain 68% and 95% of the posterior probability.

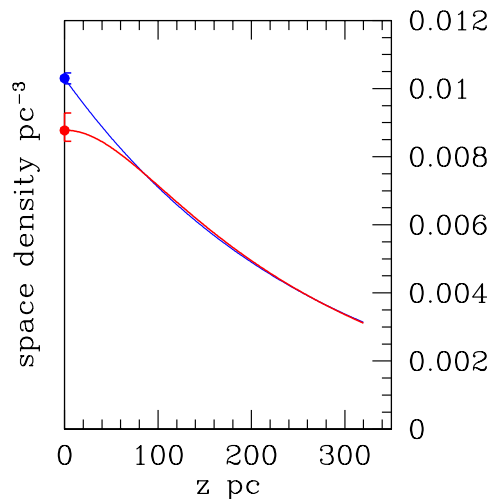


FIG. 8.— Final best-fit density profiles from the likelihood analysis, summed over M7 to L2.5:  $\text{sech}^\alpha$  (red) and exponential (blue).

for Malmquist bias, these pairs become a) [227, 0.23], b) [252, 0.26], c) [259, 0.29]. We see that accounting correctly for binaries has a substantial effect. Without allowance for binaries the scale height is underestimated by 10%. The effect of Malmquist bias is considerably smaller. If not accounted for, the scale height is underestimated by 3%. We believe this is the first time that the corrections for binaries and for Malmquist bias have been made in this direct way, as opposed to using mock catalogues.

The sign and the size of these biases are in very good agreement with the results of Jurić et al. (2008) for

the SDSS, computed using mock catalogues. For example they found (we find) that for a binary fraction  $f_b = 0.25$  (0.162) the scale height is underestimated by 15% (10%). For Malmquist bias they found (we find) that for  $\sigma_M = 0.30$  (0.24) the scale height is underestimated by  $\sim 5\%$  (3%).

Using each source individually rather than binning the data ensures that the data are used optimally. However, this has a large cost in terms of the computational time required for the fit, and the gain is actually probably rather modest. For much larger sample sizes than used here the computational cost could be prohibitive. In such cases a compromise is possible. The key would be to bin the data in  $J$  and  $b$ , rather than in  $z$ , for each spectral sub-type. Then it would still be possible to implement a likelihood treatment for binaries and Malmquist bias analogous to the one employed here.

#### 4. DISCUSSION OF THE MEASURED DENSITY PROFILE

The measured value of  $\alpha = 0.29^{+0.12}_{-0.13}$  for this population of stars corroborates the finding of Xiang et al. (2018) that  $\alpha \sim 0$  for the thin disk, summing all ages together. The result is also in good agreement with the measurement by de Grijs et al. (1997) of the distribution of  $\alpha$  in nearby edge-on spiral galaxies of  $\alpha = 0.5 \pm 0.2$ . Since these latter measurements were made in the  $K$  band the light would be dominated by cooler stars. Bovy (2017) found that the vertical profiles of A to K stars are ‘well represented by  $\text{sech}^2$  profiles’, and he measured scale heights increasing from  $\sim 50$  pc for (younger) A stars to  $\sim 150$  pc for (older) G and K dwarfs. The latter value is much smaller than the canonical value for the thin disk of 300 pc which is hard to understand. However in contrast to the A stars, the vertical profiles of G and K dwarfs are not well sampled by the GAIA DR1 data. It may be possible to reconcile all these results in the following way. The results of Xiang et al. (2018) indicate that  $\alpha$  is larger for young populations, so the profile for A stars might be satisfactorily fit by a  $\text{sech}^2$  profile. However the G and K samples will be dominated by older stars so for these populations one would expect a value of  $\alpha$  similar to our measurement of 0.29. If this is true, fitting the  $\text{sech}^2$  profile to this steeper profile will result in a substantial underestimate of the scale height, as we found in Sect. 3.1 (the same effect is also visible as the anti-correlation between  $z_e$  and  $\alpha$  in Fig. 7). This might help explain the small scale heights measured by Bovy (2017) for G and K dwarfs.

The measured value of  $\alpha$  is interesting from a theoretical perspective because it is inconsistent with the value  $\alpha = 2$  predicted for an isothermal distribution. Banerjee and Jog (2007) have argued that a steeper value would be expected as a consequence of the constraining effect of the mass in the thin gaseous disk.

The measured scale height  $z_e = 259$  pc for the  $\text{sech}^\alpha$  profile, or  $z_e = 269$  pc for the exponential profile, is broadly in line with previous measurements for the thin disk. A useful comparison is against the result of Bochanski et al. (2010) who measured a scale height of  $300 \pm 15$  pc from a large sample of early and mid M dwarfs, accounting for binaries and Malmquist bias. This is satisfactory agreement given the much larger distances sampled by their survey, the different analysis method, and the uncertainty in the photometric parallaxes used by them.

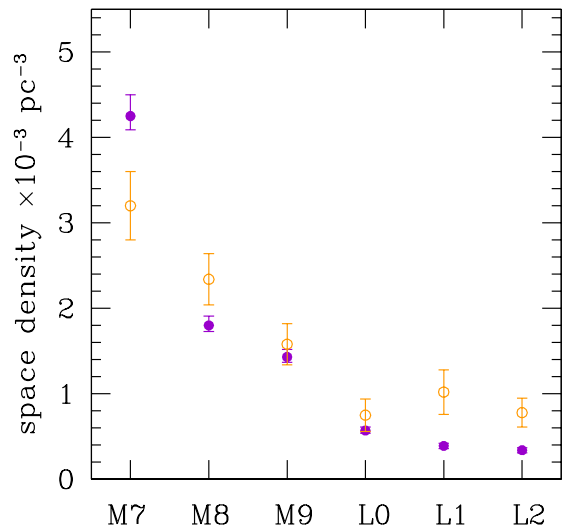


FIG. 9.— Comparison of measured local space density by spectral type. Solid points: this paper. Open points: Bardalez Gagliuffi et al. (2019).

TABLE 3  
COMPARISON OF SPACE DENSITIES  $\text{pc}^{-3}$  IN THIS PAPER AGAINST  
BARDALEZ GAGLIUFFI ET AL. (2019)

spectral type	this paper	Bardalez Gagliuffi et al. (2019)
M7	$4.25^{+0.25}_{-0.16} \times 10^{-3}$	$3.20^{+0.40}_{-0.40} \times 10^{-3}$
M8	$1.80^{+0.11}_{-0.07} \times 10^{-3}$	$2.34^{+0.30}_{-0.30} \times 10^{-3}$
M9	$1.43^{+0.09}_{-0.06} \times 10^{-3}$	$1.58^{+0.24}_{-0.24} \times 10^{-3}$
L0	$0.57^{+0.04}_{-0.03} \times 10^{-3}$	$0.75^{+0.19}_{-0.19} \times 10^{-3}$
L1	$0.39^{+0.03}_{-0.03} \times 10^{-3}$	$1.02^{+0.26}_{-0.26} \times 10^{-3}$
L2	$0.34^{+0.03}_{-0.03} \times 10^{-3}$	$0.78^{+0.17}_{-0.17} \times 10^{-3}$

The measured height of the Sun above the plane of  $10.9^{+1.7}_{-1.6}$  pc also deserves comment. There have been several measurements of this quantity. One of the most recent and most detailed is the study of Bennett and Bovy (2019) who find a height  $20.8 \pm 0.3$  pc. They emphasise the influence of asymmetries in the vertical density distribution, and they define the Galactic plane as the centre of the symmetric part of the density profile. The main asymmetry manifests itself at heights of 500 pc, beyond the limit of our survey. Since our data look symmetric we might expect the two results to agree somewhat better. Nevertheless a difference at this level has no significant effect on the estimate of  $\alpha$ .

#### 5. THE LUMINOSITY FUNCTION

The  $\text{sech}^\alpha$  fits produce an estimated space density at the Galactic plane for each spectral type, Table 2. We can now compare against measurements of the local space density, in particular the measurements by Bardalez Gagliuffi et al. (2019) who have made a comprehensive census of ultracool dwarfs at distances  $< 25$  pc. Referring to Fig. 8, with the Sun located 10 pc above the plane, the space density in the local bubble of radius 25 pc will be almost identical to the value at the mid plane.

We compare our measurements of the local space density with those of Bardalez Gagliuffi et al. (2019) in Table

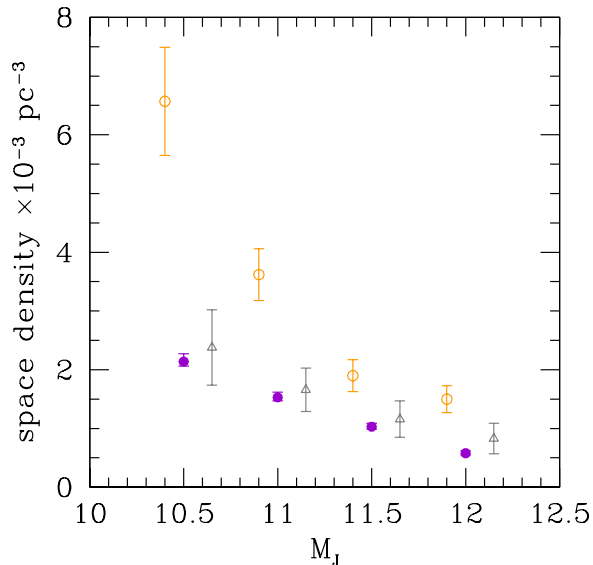


FIG. 10.— Comparison of measured luminosity functions in 0.5 mag. bins. Solid circles: this paper. Open circles: Bardalez Gagliuffi et al. (2019). Open triangles: Cruz et al. (2007). The Bardalez Gagliuffi and Cruz points have been shifted 0.1 mag. to the left because they use the 2MASS  $J$  band whereas we use the MKO  $J$  band.

TABLE 4  
COMPARISON OF THE LUMINOSITY FUNCTION  $\text{pc}^{-3}$  FROM THIS PAPER AGAINST THE SAME FROM BARDALEZ GAGLIUFFI ET AL. (2019)

$M_J$	this paper	Bardalez Gagliuffi et al. (2019)
10.25 – 10.75	$2.14^{+0.13}_{-0.08} \times 10^{-3}$	$6.57^{+0.92}_{-0.92} \times 10^{-3}$
10.75 – 11.25	$1.53^{+0.09}_{-0.06} \times 10^{-3}$	$3.62^{+0.44}_{-0.44} \times 10^{-3}$
11.25 – 11.75	$1.03^{+0.06}_{-0.04} \times 10^{-3}$	$1.90^{+0.27}_{-0.27} \times 10^{-3}$
11.75 – 12.25	$0.58^{+0.04}_{-0.03} \times 10^{-3}$	$1.50^{+0.23}_{-0.23} \times 10^{-3}$

3 and Fig. 9. Because Bardalez Gagliuffi et al. (2019) use a full spectral sub-type, for e.g. M7 we have combined our results for M7 and M7.5.<sup>2</sup> There is mostly fair agreement between the two determinations, although the points for M7, L1, and L2 are not in statistical agreement (outside  $2\sigma$ ). For the M7 to M9 dwarfs, recall (Sect. 2) that Laithwaite and Warren (2020) noted an apparent discrepancy between spectral classifications in the homogeneous BOSS sample of Schmidt et al. (2015) and classifications collected from older literature. The difference is in the sense that older measurements found earlier spectral types than measured by Schmidt et al. (2015). If the classifications in Bardalez Gagliuffi et al. (2019) are systematically different to the BOSS classifications for M7 to M9 this would translate to differences in their measured space densities compared to ours.

The differences in space density at L1 and L2, where we measure values a factor two smaller than Bardalez Gagliuffi et al. (2019), are harder to understand. The uncertainties plotted on our sample are very small com-

<sup>2</sup> This could in principle lead to small differences. A full sub-type bin effectively covers M6.5 to M7.5. Adding two half sub-type bins effectively covers M6.75 to M7.75.

pared to theirs.

Any systematic differences in the spectral classifications between samples would not necessarily translate into differences in the measured luminosity function, as long as absolute magnitudes have been determined correctly for each sample (this would not be the case if the same relation between spectral type and absolute magnitude were used for both samples). To calculate the luminosity function we consider the bins of size 0.5 mag listed in Table 4 and compute the space density in each bin.<sup>3</sup> It is important to allow correctly for the spread in absolute magnitude of each spectral sub-type, to include all sub-types that contribute to a bin (given the spread), and to ignore bins where sub-types not considered here would contribute significantly. The last is true for example for the bin 9.75 – 10.25, where M6.5 stars would contribute. We assume the absolute magnitudes of each of the twelve spectral sub-types are centred on the values listed in Table 1 and are Gaussian distributed with  $\sigma_M = 0.24$  (Sect. 3.2.1). We then integrate the space densities in the MCMC chains into the relevant absolute magnitude bins to compute the luminosity function and uncertainties. For the highest luminosity bin 10.25 – 10.75 any contribution from spectral type M6.5 will be negligible. For the lowest luminosity bin 11.75 – 12.25 we have added in a small contribution from L3 dwarfs of  $0.02 \text{ pc}^{-3}$ , estimated by assuming the space density of L3 dwarfs is the same as that of L2.5 dwarfs.

The results are listed in Table 4, where they are compared against the luminosity function results of Bardalez Gagliuffi et al. (2019). Again we find that the uncertainties quoted by Bardalez Gagliuffi et al. (2019) are smaller than a fractional uncertainty of  $1/\sqrt{N}$ , and so the values quoted in Table 4 use  $1/\sqrt{N}$ . Our values for the luminosity function are a factor of two to three lower than those of Bardalez Gagliuffi et al. (2019). Substantially lower space densities in each bin could have been anticipated, since the estimated space densities are lower for most spectral types, Fig. 9, and in addition the range of absolute magnitudes for what we call M7 to M9 is larger than their range, so the space density per 0.5 mag. bin is further lowered for our sample. The two estimates of the luminosity function are plotted in Fig. 10. Our results use the MKO  $J$  band whereas they use the 2MASS  $J$  band. Over this spectral range a star has  $J_{2MASS} - J_{MKO} \sim 0.1$  mag. (Stephens and Leggett 2004). Therefore we have shifted their points 0.1 mag to the left in Fig. 10 to represent their results on the MKO system.

In Fig. 9 we also plot the older results on the luminosity function from Cruz et al. (2007) (their Table 11) which the Bardalez Gagliuffi et al. (2019) results supersede. These also use the 2MASS  $J$  band and so the points have also been offset to the left by 0.1 mag (their locations are plotted incorrectly in Bardalez Gagliuffi et al. (2019), offset by 0.25 mag.). Interestingly our results and those of Cruz et al. (2007) agree well.

## 6. SUMMARY

The main points in this paper are the following:

<sup>3</sup> These have been chosen to match the bins in Bardalez Gagliuffi et al. (2019). We have been informed that where they list a bin as 10.25, this means the range 10.25 – 10.75.

1. We have used a homogeneous sample of 34 000 ultracool dwarfs of spectral type M7 to L2.5, all at distances  $< 350$  pc, to measure the local vertical density distribution of stars in the disk of the Milky Way. The sample was selected in the  $J$  band and benefits from high photometric precision and low extinction. We have developed a likelihood analysis that uses all the stars in the sample optimally, accounting directly for the proportion of unresolved binaries in the sample, and treating Malmquist bias.
2. Fitting the function  $\text{sech}^\alpha$  to the density distribution as a function of height from the Galactic plane, we measure  $\alpha = 0.29^{+0.12}_{-0.13}$ . The exponential profile  $\alpha = 0$  is contained within the 95% credible interval. Any softening of the density distribution towards the plane relative to an exponential profile is modest. The flatter  $\text{sech}$  and  $\text{sech}^2$  profiles are ruled out at high confidence.
3. Because of the good sampling of the peak of the density distribution the sample is useful for measuring the location of the Galactic plane for this population, and we find the Sun lies at a height  $10.9^{+1.7}_{-1.6}$  pc above the plane.
4. We have used the results of the fit of the density profile to measure the stellar luminosity function at the bottom of the main sequence over the absolute magnitude interval  $10.25 < M_J < 12.25$ . Our results for the luminosity function are a factor two to three lower than the measurements by Bardalez Gagliuffi et al. (2019) that uses stars in the local 25 pc radius bubble, but agree well with the older study of Cruz et al. (2007).

## ACKNOWLEDGEMENTS

We are grateful to Daniel Mortlock for a number of helpful discussions on data analysis, and to Daniella Bardalez Gagliuffi for comments on an earlier version of the manuscript.

## REFERENCES

- Ahmed, S., and Warren, S. (2019), “A homogeneous sample of 34 000 M7- M9. 5 dwarfs brighter than  $J= 17.5$  with accurate spectral types,” *Astronomy & Astrophysics*, 623, A127.
- Banerjee, A., and Jog, C. J. (2007), “The Origin of Steep Vertical Stellar Distribution in the Galactic Disk,” *The Astrophysical Journal*, 662, 335–340.
- Bardalez Gagliuffi, D. C., Burgasser, A. J., Schmidt, S. J., Theissen, C., Gagné, J., Gillon, M., Sahlmann, J., Faherty, J. K., Gelino, C., Cruz, K. L., Skrzypek, N., and Looper, D. (2019), “The Ultracool SpeXtoscopic Survey. I. Volume-limited Spectroscopic Sample and Luminosity Function of M7-L5 Ultracool Dwarfs,” *ApJ*, 883(2), 205.
- Bennett, M., and Bovy, J. (2019), “Vertical waves in the solar neighbourhood in Gaia DR2,” *MNRAS*, 482(1), 1417–1425.
- Bochanski, J. J., Hawley, S. L., Covey, K. R., West, A. A., Reid, I. N., Golimowski, D. A., and Ivezić, Z. (2010), “The Luminosity and Mass Functions of Low-mass Stars in the Galactic Disk. II. The Field,” *The Astronomical Journal*, 139(6), 2679–2699.
- Bovy, J. (2017), “Stellar Inventory of the Solar Neighborhood using Gaia DR1,” *Monthly Notices of the Royal Astronomical Society*, 470, 1360–1387.
- Camm, G. L. (1950), “Self-gravitating star systems,” *MNRAS*, 110, 305.
- Chang, C.-K., Ko, C.-M., and Peng, T.-H. (2011), “Information on the Milky Way from the Two Micron All Sky Survey Whole Sky Star Count: The Structure Parameters,” *The Astrophysical Journal*, 740(1).
- Covey, K. R., Hawley, S. L., Bochanski, J. J., West, A. A., Reid, I. N., Golimowski, D. A., Davenport, J. R. A., Henry, T., Uomoto, A., and Holtzman, J. A. (2008), “The Luminosity and Mass Functions of Low-Mass Stars in the Galactic Disk. I. The Calibration Region,” *AJ*, 136(5), 1778–1798.
- Cruz, K. L., Reid, I. N., Kirkpatrick, J. D., Burgasser, A. J., Liebert, J., Solomon, A. R., Schmidt, S. J., Allen, P. R., Hawley, S. L., and Covey, K. R. (2007), “Meeting the Cool Neighbors. IX. The Luminosity Function of M7-L8 Ultracool Dwarfs in the Field,” *AJ*, 133(2), 439–467.
- de Grijis, R., Peletier, R., and van der Kruit, P. (1997), “The z-structure of disk galaxies towards galactic planes,” *Astronomy and Astrophysics*, 327, 966–982.
- Dieterich, S. B., Henry, T. J., Jao, W.-C., Winters, J. G., Hosey, A. D., Riedel, A. R., and Subasavage, J. P. (2014), “The Solar Neighborhood. XXXII. The Hydrogen Burning Limit,” *AJ*, 147(5), 94.
- Dobbie, P. S., and Warren, S. J. (2020), “A Bayesian Approach to the Vertical Structure of the Disk of the Milky Way,” *The Open Journal of Astrophysics*, 3(1), 5.
- Dupuy, T. J., and Liu, M. C. (2012), “The Hawaii Infrared Parallax Program. I. Ultracool Binaries and the L/T Transition,” *ApJS*, 201(2), 19.
- Ferguson, D., Gardner, S., and Yanny, B. (2017), “Milky Way Tomography with K and M Dwarf Stars: The Vertical Structure of the Galactic Disk,” *The Astrophysical Journal*, 843(2).
- Foreman-Mackey, D., Hogg, D. W., Lang, D., and Goodman, J. (2013), “emcee: The MCMC Hammer,” *PASP*, 125(925), 306.
- Gilmore, G., and Reid, N. (1983), “New light on faint stars. III - Galactic structure towards the South Pole and the Galactic thick disc,” *Monthly Notices of the Royal Astronomical Society*, 202(March), 1025–1047.
- Gould, A., Bahcall, J. N., and Flynn, C. (1996), “Disk M Dwarf Luminosity Function from Hubble Space Telescope Star Counts,” *ApJ*, 465, 759.
- Green, G. M., Schlafly, E. F., Finkbeiner, D., Rix, H.-W., Martin, N., Burgett, W., Draper, P. W., Flewelling, H., Hodapp, K., Kaiser, N., Kudritzki, R.-P., Magnier, E. A., Metcalfe, N., Tonry, J. L., Wainscoat, R., and Waters, C. (2018), “Galactic reddening in 3D from stellar photometry - an improved map,” *MNRAS*, 478(1), 651–666.
- Hammersley, P. L., Cohen, M., Garzón, F., Mahoney, T., and López-Corrodoira, M. (1999), “Structure in the first quadrant of the Galaxy: an analysis of TMGS star counts using the SKY model,” *MNRAS*, 308(2), 333–363.
- Jurić, M., Ivezić, Z., Brooks, A., Lupton, R. H., Schlegel, D., Finkbeiner, D., Padmanabhan, N., Bond, N., Sesar, B., Rockosi, C. M., Knapp, G. R., Gunn, J. E., Sumi, T., Schneider, D. P., Barentine, J. C., Brewington, H. J., Brinkmann, J., Fukugita, M., Harvanek, M., Kleinman, S. J., Krzesinski, J., Long, D., Neilsen, E. H. J., Nitta, A., Snedden, S. A., and York, D. G. (2008), “The Milky Way Tomography with SDSS. I. Stellar Number Density Distribution,” *The Astrophysical Journal*, 673(2), 864–914.
- Kirkpatrick, J. D., Reid, I. N., Liebert, J., Cutri, R. M., Nelson, B., Beichman, C. A., Dahn, C. C., Monet, D. G., Gizis, J. E., and Skrutskie, M. F. (1999), “Dwarfs Cooler than ‘M’: The Definition of Spectral Type ‘L’ Using Discoveries from the 2 Micron All-Sky Survey (2MASS),” *ApJ*, 519(2), 802–833.
- Laithwaite, R. C., and Warren, S. J. (2020), “The absolute magnitudes  $M_J$ , the binary fraction, and the binary mass ratios of M7 to M9.5 dwarfs,” *arXiv e-prints*, p. arXiv:2006.11092.
- Lewis, A. (2019), “GetDist: a Python package for analysing Monte Carlo samples,” *arXiv e-prints*, p. arXiv:1910.13970.
- Marshall, H. L., Tananbaum, H., Avni, Y., and Zamorani, G. (1983), “Analysis of complete quasar samples to obtain parameters of luminosity and evolution functions,” *ApJ*, 269, 35–41.

- Reid, I. N., Cruz, K. L., Burgasser, A. J., and Liu, M. C. (2008), “L-Dwarf Binaries in the 20-Parsec Sample,” *AJ*, 135(2), 580–587.
- Schmidt, S. J., Hawley, S. L., West, A. A., Bochanski, J. J., Davenport, J. R. A., Ge, J., and Schneider, D. P. (2015), “BOSS Ultracool Dwarfs. I. Colors and Magnetic Activity of M and L Dwarfs,” *AJ*, 149(5), 158.
- Siegel, M. H., Majewski, S. R., Reid, I. N., and Thompson, I. B. (2002), “Star Counts Redivivus. IV. Density Laws through Photometric Parallaxes,” *The Astrophysical Journal*, 578(1), 151–175.
- Skrzypek, N., Warren, S. J., and Faherty, J. K. (2016), “Photometric brown-dwarf classification. II. A homogeneous sample of 1361 L and T dwarfs brighter than  $J = 17.5$  with accurate spectral types,” *A&A*, 589, A49.
- Skrzypek, N., Warren, S. J., Faherty, J. K., Mortlock, D. J., Burgasser, A. J., and Hewett, P. C. (2015), “Photometric brown-dwarf classification. I. A method to identify and accurately classify large samples of brown dwarfs without spectroscopy,” *A&A*, 574, A78.
- Spitzer, L. (1942), “The Dynamics of Interstellar Medium III. Galactic Distribution,” *The Astrophysical Journal*, 95(3), 329.
- Stephens, D. C., and Leggett, S. K. (2004), “JHK Magnitudes for L and T Dwarfs and Infrared Photometric Systems,” *PASP*, 116(815), 9–21.
- Tokunaga, A. T., Simons, D. A., and Vacca, W. D. (2002), “The Mauna Kea Observatories Near-Infrared Filter Set. II. Specifications for a New JHKL’M’ Filter Set for Infrared Astronomy,” *PASP*, 114(792), 180–186.
- Van der Kruit, P. (1988), “The three-dimensional distribution of light and mass in disks of spiral galaxies,” *Astronomy and Astrophysics*, 192(1-2), 117–127.
- van der Kruit, P. C., and Searle, L. (1981), “Surface photometry of edge-on spiral galaxies. I - A model for the three-dimensional distribution of light in galactic disks,” *A&A*, 95, 105–115.
- Widrow, L. M., Gardner, S., Yanny, B., Dodelson, S., and Chen, H.-Y. (2012), “Galactoseismology: discovery of vertical waves in the Galactic Disk,” *The Astrophysical Journal Letters*, 750(2), L41.
- Xiang, M., Shi, J., Liu, X., Yuan, H., Chen, B., Huang, Y., Wang, C., Wu, Y., Tian, Z., Huo, Z., Zhang, H., and Zhang, M. (2018), “Stellar Mass Distribution and Star Formation History of the Galactic Disk Revealed by Mono-age Stellar Populations from LAMOST,” *ApJS*, 237(2), 33.